

Freestanding carbon nanodots/poly (vinyl alcohol) films with high photoluminescent quantum yield realized by inverted-pyramid structure

Linna Pang, Lixiang Ba, Wei Pan¹ and Wenzhong Shen¹

Laboratory of Condensed Matter Spectroscopy and Opto-Electronic Physics, and Key Laboratory of Artificial Structures and Quantum Control (Ministry of Education), Department of Physics and Astronomy, Shanghai Jiao Tong University, Shanghai 200240, People's Republic of China

E-mail: sjtushelwill@sjtu.edu.cn and wzshen@sjtu.edu.cn

Received 7 October 2016, revised 14 December 2016

Accepted for publication 5 January 2017

Published 25 January 2017



CrossMark

Abstract

Carbon nanodots (C-dots) have attracted great attention for their biocompatibility and strong tunable photoluminescence (PL). However, aggregation-induced PL quenching blocks their practical application in solid-state optoelectronics. Here, we report a luminescent C-dots freestanding film with a substantially enhanced high quantum yield (QY) of 72.3%. A facile template method, rather than complicate lithography and etching technique is proposed to fabricate the C-dots composite films with large-area (8 inch \times 8 inch) ordered micro-scale inverted-pyramid patterns on the surface. The control experiment and theoretical analysis demonstrate the key success to QY enhancement lies in the separation of C-dots and the pattern of surface inverted-pyramid structure. This work realizes the QY enhancement simply by geometrical optics, not the chemical treatment of luminescent particles. It provides a general approach to fabricate large-area freestanding luminescent composite film with high QY.

Supplementary material for this article is available [online](#)

Keywords: inverted-pyramid structure, composite films, carbon nanodots, high photoluminescent quantum yield

(Some figures may appear in colour only in the online journal)

1. Introduction

Solution-phase semiconductor quantum dots, including Cd-based and carbon nanomaterials, have been regarded as promising alternatives for conventional organic fluorophores because of their photo-stability and high brightness [1–3]. Among them, carbon nanodots (C-dots) have attracted great attention since first synthesized in 2006 due to their low toxicity and excellent biocompatibility [4, 5], low-cost and readily available abundant raw materials [6, 7], facile synthesis [8, 9], and especially the strong and tunable

photoluminescence (PL) spanning the whole visible spectrum [10, 11]. These C-dots provide great opportunities in device applications, such as bioimaging, optical sensing, light emitting diode and other optoelectronic devices [3, 12, 13]. However, up to now, most previous studies about C-dots were performed in their original aqueous solution, and only few reports were concentrated on the exploration of their solid-state photo-physical properties due to the limitation of aggregation-induced PL quenching [14, 15].

The main strategies to enhance PL of C-dots films include the surface modification [7, 9, 16] and the incorporation of them in polymer or inorganic matrix [12–14, 17] to protect and disperse the C-dots. Embedding C-dots in

¹ Authors to whom any correspondence should be addressed.

polymer not only provides particle protection and dispersion, but produces a freestanding film [14, 18, 19], so that this approach is widely adopted. Due to the planar structure and the larger refractive index of the polymer, the embedment of C-dots in polymer brings the waveguide-mode losses, which obviously weakens the quantum yield (QY) of the C-dots/polymer composite films. In order to prevent it, Jiang *et al* [20] recently patterned submicron-scale Bragg gratings structure on the surface of C-dots composite films, to extract the waveguide-mode light. The protection and dispersion of luminescent center, together with the submicron-scale Bragg gratings structure, help to enhance the QY of solid C-dots thin films to ~60% [20–22]. However, compared to the QY (>90%) of C-dots aqueous solution [23], there is still much room for QY improvement of the C-dots film. Besides, the increase of PL was frequently accompanied by the change in emission wavelength [12, 24]. Hence, it is still challenging for us to effectively fabricate the C-dots films with higher QY and exploit their optical physical properties.

In this work, we report a blue-emitting C-dots embedded freestanding film patterned with large-area (8 inch × 8 inch) ordered micron-scale inverted-pyramid structure with a QY of 72.3%. Simulation with the algorithm of finite-difference time-domain (FDTD) firstly demonstrates the facilitation of inverted-pyramid structure to light extraction. A facile template method is then used to fabricate the C-dots composite films with large-area ordered inverted-pyramid patterns by using a surface micro-textured silicon wafer as a template. As-prepared C-dots exhibits an obviously enhanced QY of 72.3%, almost equivalent to that of C-dots counter-original aqueous solution. The control experiment and theoretical analysis further illustrate that this dramatic QY enhancement mainly comes from the magnification of light output induced by geometric structure. This work provides a general and facile approach to fabricate large-area freestanding luminescent composite film with liquid-comparably high PL QY by simply optimizing the geometrical optics, rather than traditional chemical treatment of luminescent particles.

2. Experimental section

2.1. C-dots/PVA films fabrication

The C-dots were synthesized from citric acid, ammonia water, and ethylene diamine via a previously reported hydrothermal method [25]. After synthesis, the poly (vinyl alcohol) (PVA) powder was introduced into the C-dots diluted solution, and then stirred for a couple of hours at 90 °C to form the well-dispersed solution. The obtained mixture was centrifuged at 6000 rounds per minute to expel air inside and subsequently dropped on home-made moulds. The moulds containing C-dots/PVA solution was low-temperature heated (35 °C–40 °C) for several hours, and then a large-area freestanding C-dots/PVA composite film was obtained by peeling it off the moulds carefully. The film thickness was controlled by the injection volume of the original solution. To realize the inverted-pyramid surface, the microstructured silicon wafer

was prepared by a common base etching procedure [26] and then placed in the moulds to act as template.

2.2. Characterization

The high resolution transmission electron microscopy images were obtained by a JEOL (Japan) JEM-2100F TEM. The ultraviolet–visible (UV–vis) absorption spectra were measured by a Perkin-Elmer (USA) Lambda 20 spectrometer. The steady state PL spectra of C-dots aqueous solution and C-dots/PVA composite films were recorded by using a fluorescence spectrofluorometer equipped with an integrating sphere accessory (Horiba Jobin Yvon, FL, Japan). The temperature-dependent fluorescence decay spectra of C-dots/PVA composite films were performed by time-resolved fluorescence spectrofluorometer (QM/TM/IM, PTI, USA) with a variable temperature liquid nitrogen cryostat accessory (Oxford Instrument, UK). The morphology and thickness of C-dots/PVA composite films were examined by a Zeiss (Germany) ultra plus field-emission scanning electron microscopy (SEM). The simulations in this work were performed using a commercial software package (FDTD Solution v8, Lumerical 2013).

3. Results and discussion

As-prepared water-soluble C-dots exhibit the high crystallinity (shown in figure S1) with a lattice parameter of 0.243 nm, close to the in-plane lattice spacing (0.250 nm) of graphene. They exhibit absorption peaks at 238 and 348 nm (dark cyan), and emits blue fluorescence (orange, 440 nm PL peak) with the corresponding PL excitation (PLE) peak (black line) locating at 353 nm, as shown in figure S2. QY measurements shown in figure S3 illustrate that diluted C-dots aqueous solution (absorbance < 0.05) has a relative QY value of 87.3% with quinine sulfate as a QY standard reference. However, as displayed in figure S4, QY decreases dramatically with the increase of C-dots concentration and the corresponding absorbance, suggesting the existence of typical aggregation-induced PL quenching. To prevent further aggregation and thus PL quenching in the fabrication process of C-dots film, highly transmitted PVA were introduced as matrix to separate and protect the fluorescent C-dots, as reported elsewhere [12, 18, 20].

The direct embedment of C-dots into PVA is easy to induce waveguide-mode losses of the light. To avoid it, surface microstructure has been used to extract the internal light [27–31], including the submicron-scale Bragg gratings to enhance the diffraction [28, 29] and the designed micron-scale microstructure to weaken the total internal reflection [30, 31]. The inverted-pyramid structure, which has been applied on the solar cell to promote the absorption, is considered to be able to alter the incident angle of the reflected internal light, compress waveguide-mode losses, and thus enhances the light output of the film. To testify it, the absorption and light output of the film with smooth surface (SS) and inverted-pyramid surface (IPS) were simulated firstly via the method of FDTD, as shown in figure 1. In the

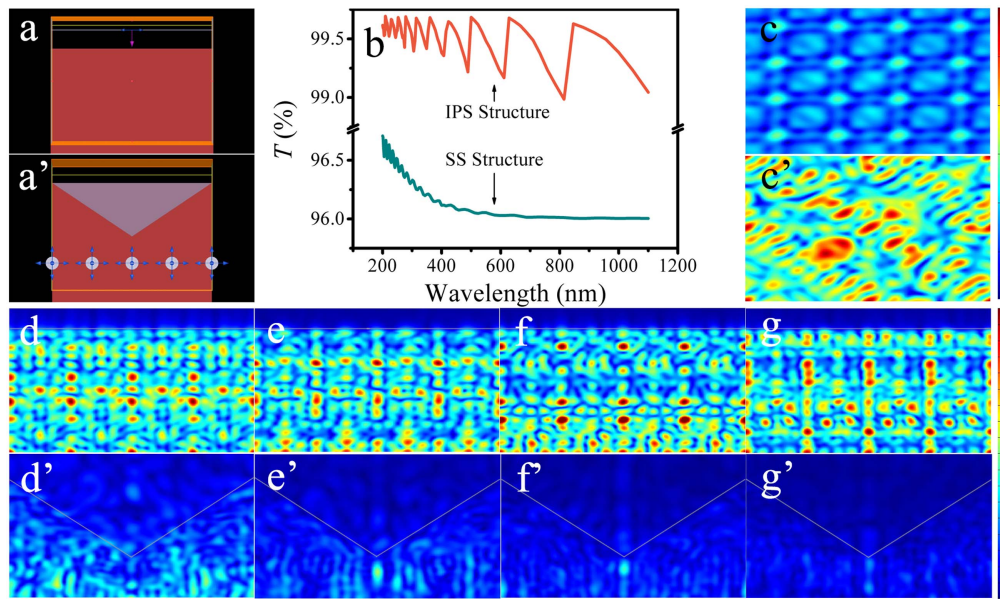


Figure 1. Graphic presentation of FDTD simulation for (a) absorption and (a') emission of SS and IPS C-dots/PVA film. (b) FDTD simulated light transmission rate T through SS (dark cyan line) and IPS (orange line) structure in a range of 200–1100 nm. Top view of time-integrated light intensity distribution of (c) SS film and (d) IPS film. Sectional view of light intensity distribution in (d)–(g) SS film and (d')–(g') IPS film detected at 500 (d), (d'), 1000 (e), (e'), 1500 (f), (f') and 2000 (g), (g') fs respectively.

simulation, the facet tilt angle and height of the inverted-pyramid were set as 51° and $2 \mu\text{m}$ according to the previous reports [32, 33].

Figures 1(a) and (a') show the graphic presentation of simulation for absorption (a) and light output (a') of SS and IPS films, respectively. For absorption, the plane wave irradiates along minus- z direction perpendicular to the film, and the light reflected by film surface was recorded by a frequency-domain transmission monitor set above the simulated region parallel to surface. The obtained transmission rate T (figure 1(b)) through the IPS oscillates around 99.5% throughout the whole UV–vis spectrum, a little higher than that through SS (highest to 96.5% at deep UV and stabilized at 96% in visible region). It suggests a lower light reflection induced by the IPS structure. For light output simulation (figure 1(a')), due to the limitation of computer memory, the uniformly dispersed fluorescent C-dots were simplified as regularly arranged matrix (with 800 nm intervals) of TE/TM dipoles placed at a plane $3 \mu\text{m}$ below the surface. PVA, as the main composition of the film, was set to be a material with a refractive index of 1.5 and an extinction coefficient of 0. Two monitors were set, one above the film surface to record light intensity extracted from film, and the other perpendicular to the film surface to detect the light intensity inside the film. Apparently, the overall intensity of light emitting from SS film (figure 1(c)) is quite low, in sharp contrast to greatly amplified light intensity over the monitored area from IPS film (figure 1(c')). It indicates the IPS structure is advantageous to the light extraction, which is also supported by the time-dependent light intensity distribution inside the film. Figures 1(d)–(g') display the section views of light intensity distribution detected at 500, 1000, 1500, and 2000 fs, respectively. For comparison, the light intensity in these

figures has been normalized to a same scale. Observably, the light intensity inside the IPS film decreases sharply with the elapse of time, and is barely any after 2000 fs. However, the light intensity inside SS film virtually remains at the same level, exhibiting an obvious waveguide effect. Therefore, it is easy to make the conclusion that IPS can help to overcome the waveguide loss and to extract almost all the light inside the film. Patterning inverted-pyramid structure on the C-dots/PVA films will be a good strategy to fabricate the free-standing C-dots/PVA films with high QY.

The procedure of film fabrication is shown in figure 2. Simply speaking, the mixture of PVA and C-dots aqueous solution was introduced into a home-made mould and then dried in air to form a freestanding C-dots/PVA composite film with IPS structure (figure 2(a)). For convenience, not the complicated lithography and etching technique, but a facile template method was utilized to pattern the large-area (8 inch \times 8 inch) ordered micron-scale inverted-pyramid structures on the surface of C-dots/PVA films. The template was fabricated by a common industry method, etching the 8 inch silicon wafer with base solution [26]. Despite of its simplicity, the template method is efficient to fabricate the film with IPS patterns. The cross-section SEM image of a typical IPS film in figure 2(b) suggests the existence of surface microstructure. The corresponding top-view and tilted-angle-view SEM images in figure S5 further demonstrate the micron-scale inverted-pyramid surface. Statistics analysis of SEM images indicates these inverted-pyramids have an average bottom width of $3.2 \pm 1.1 \mu\text{m}$, height of $2.0 \pm 0.6 \mu\text{m}$, and facet tilt angle of $50.5 \pm 1.3^\circ$, as shown in the insets of figure S5(b). The successful realization of IPS films is expected to help enhance the output of light inside the film, as predicted by the

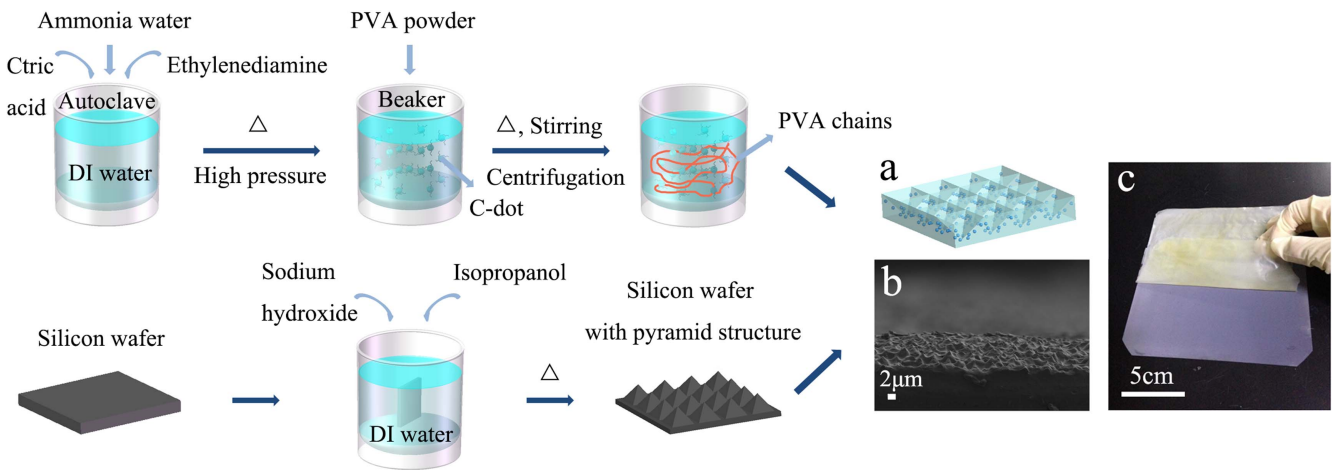


Figure 2. Schematic diagram for the fabrication of the C-dots/PVA films. (a) Schematic figure, (b) cross-section SEM image, and (c) digital photo of IPS film.

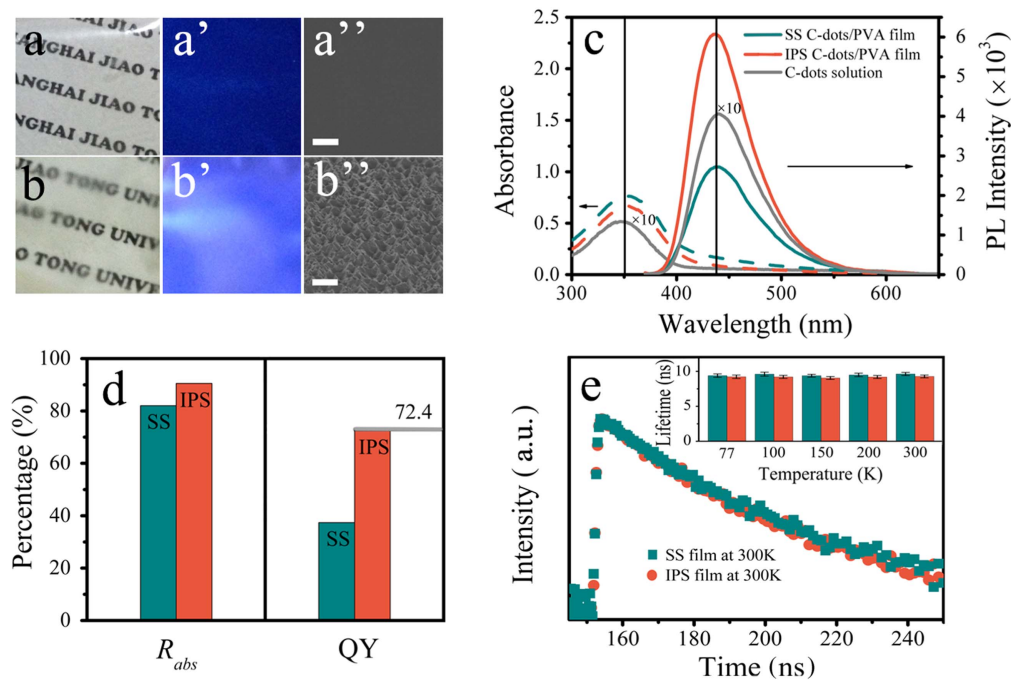


Figure 3. Photos of C-dots/PVA film with (a), (a') SS and (b), (b') IPS under (a), (b) room light and (a'), (b') 365 nm UV light. SEM images of C-dots/PVA film with (a'') SS and (b'') IPS. The scale bar is 2 μm . (c) Absorption and PL (excited at 350 nm) spectra of C-dot aqueous solution and C-dots/PVA films. (d) Calculated absorption rate (left) and absolute QY (right) of C-dots/PVA films. The gray line in the figure represents the QY of the counter-original C-dots aqueous solution. (e) PL decay spectra (detected at 440 nm with 350 nm excitation) of the C-dots/PVA films at 300 K. Inset shows the corresponding extracted lifetimes at different temperatures. The color of gray, orange, and dark cyan in Figures (c)–(e) represents the C-dots aqueous solution, C-dots/PVA films with SS and IPS respectively.

FDTD simulation. For comparison, the C-dots/PVA films with SS were also fabricated in the same condition.

Figures 3(a)–(b') show the digital photos of the fabricated C-dots/PVA composite films with and without IPS patterns, whose difference in morphology can be observed in details from SEM images in figures 3(a'') and (b''). As displayed in these figures, the C-dots/PVA composite films are transparent under room light (figures 3(a) and (b)) and emit blue luminescence (figures 3(a') and (b')) under UV (360 nm)

illumination, in spite of the different SS (figure 3(a'')) and IPS surface (figure 3(b'')). Compared to the SS film, the IPS film shows frosted texture under room light, and apparently brighter blue light under UV illumination. The optical characterization (figure 3(c)) further illustrates that the C-dots/PVA composite films, with either SS or IPS, still absorb ~ 350 nm UV photons and convert them into ~ 440 nm blue emission, as same as the original C-dots aqueous solution. These facts indicate that the C-dots/PVA composite films

preserve the basic optical properties of original C-dots aqueous solution, which facilitates the direct application of C-dots from aqueous solution to composite thin film. Figure 3(c) also demonstrates that the absorbance of IPS film is a little higher than that of SS film, but its fluorescence intensity is about two times of that of SS film when excited at 350 nm with the same intensity. Here, to exclude the scattering effect, the above absorption and PL spectra of the C-dots/PVA films were measured via an integrating sphere, which guarantees the collection of all the scattered and emergent light of the sample. According to the spectra (figure S6) detected with and without the sample inside the integrating sphere, the absorption rate (R_{abs}) and absolute QY were accurately calculated by the photon counts absorbed and emitted, as shown in figure 3(d). Obviously, the IPS film exhibits better optical properties. Its R_{abs} is nearly 10% higher than that of SS film and its QY bounces up to 72.3%, about twice of that of SS film (37.4%). More importantly, compared to the reported highest QY value of $\sim 60\%$ for C-dots films [21, 22], the QY of IPS film exhibits a substantially increased value.

The FDTD simulation in figure 1 has indicated that compared to planar structure, IPS structure is helpful to extract all the light inside, and thus enhances the QY of the film. However, the enhancement of QY in IPS film could not be simply attributed to the contribution of IPS structure, since QY of the film is related to not only the emitting and absorbed light, but the QY of C-dots particles inside. Hence, PL decay curves at different temperatures (77, 100, 150, 200, and 300 K) were also detected at 440 nm with an excitation of 350 nm. As shown in figures 3(e) and S7, these PL decay curves of both SS and IPS film at different temperatures exhibit an identical mono-exponential PL decay behavior. The little discrepancy of the extracted lifetime (shown in the inset of figure 3(e)) illustrates the same recombination process, indicating no new chemical bond was form in IPS film. Therefore, the remarkable QY enhancement of IPS film mainly comes from the magnification of light extraction induced by inverted-pyramid structure. Besides, the QY of IPS film is almost equivalent to that (72.4%) of counter-original aqueous solution, although the density of C-dots in IPS films is about one hundred times of that in the original aqueous solution. This phenomenon indicates that in IPS film, not only waveguide-mode losses, but aggregation-induced PL quenching has been compressed.

In order to validate the accuracy of the above conclusion, and also comprehend the influence of fabrication parameters, a series of control experiments were carried out. The SS and IPS composite films were firstly prepared from C-dots/PVA solution of different concentrations (50, 100, 200 and 400 μl for every 10 ml to manage 0.5%, 1%, 2%, and 3% volume fraction of the as-prepared C-dots to PVA aqueous solution). Their QY, together with that of counter-original solution (marked by gray dots), are given in figure 4(a). Obviously, IPS films always possess a greater QY value, about two times of that in SS films and especially, almost reaching the level of the original C-dots aqueous solution, even though the particle

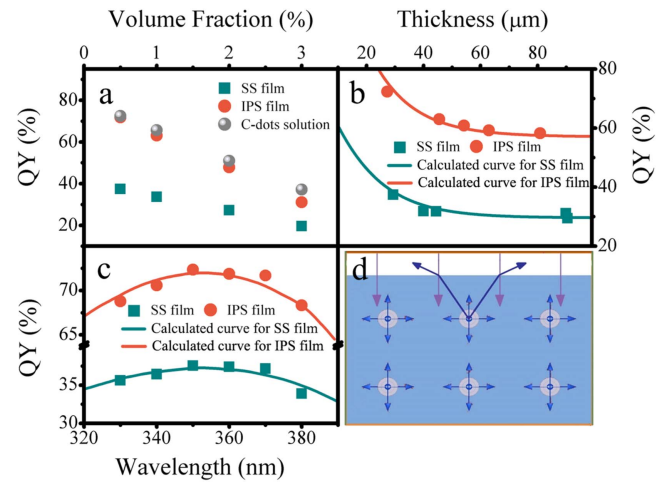


Figure 4. QY (excited at 350 nm) of C-dots/PVA film with SS (dark cyan) and IPS (orange) (a) made from solution of different volume fraction of as-prepared C-dots to PVA aqueous solution, (b) with different thicknesses, and (c) excited with different wavelengths. (d) Schematic diagram of analytical simulation for the C-dots/PVA thin film. The gray dots in (a) mark the QY of counter-original C-dots aqueous solution. Blue cyan and orange line in (b) and (c) show the calculated result for SS and IPS film respectively.

density is about a hundredfold higher. Furthermore, with the increasing concentration of the original solution, the QY of the films (both IPS and SS film) is declining as that of C-dots/PVA aqueous solution. It implies the as-prepared films prevents further particles aggregation in the film, although they are unavoidably affected by the particle aggregation in the original solution. Due to the waveguide loss in SS film, the efficiency of light extraction in IPS film is much higher than that in SS film, and the QY of IPS film exhibits a faster decline.

By using the C-dots aqueous solution with less particle aggregation (0.5% volume fraction), further experiments were performed to study the effect of film thickness and excitation wavelength. As shown in figures 4(b) and (c), QY of IPS films still exhibits a substantial gap with that of SS film. Simultaneously, QY of C-dots composite films displays a decay tendency with the growing thickness and finally reaches a relatively steady value. When excited with different wavelengths, the variation of QY of the films is in accordance with that of absorbance measured in the integrated sphere (figure 3(b)). To illustrate this variation, a theoretical model was proposed. As shown in figure 4(d), when light with the intensity of I_0 is illuminated on the C-dots/PVA films, it will be absorbed by C-dots with a wavelength-dependent absorption coefficient of α_1 . The C-dots, located at the plane with a distance of x away from the surface, absorb the light with an intensity of $I_0 \exp(-\alpha_1 nx) (\alpha_1 n) dx$, where n is the concentration of C-dots. The absorbed light is converted into emission with an intensity of $I_0 \exp(-\alpha_1 nx) (\alpha_1 n) \exp(-\alpha_2 nx / \cos(\theta)) dx$ at an arbitrary emergent angle θ , where α_2 represents the extinction coefficient of light induced by absorption and scattering. Accordingly, the QY of the film could be

Table 1. The absolute QY of original aqueous solution, SS film and IPS film embedding urea-made C-dots and quinine sulfate.

	Urea-made C-dots	Quinine sulfate
Original aqueous solution	53.7%	57.7%
SS film	29.0%	34.6%
IPS film	53.6%	57.5%

calculated from the formula below

$$\begin{aligned}
 \text{QY} = \frac{I_{\text{em}}}{I_{\text{abs}}} = & \frac{\alpha_1}{\pi [1 - \exp(-\alpha_1 nd)]} \\
 & \times \int_0^{\sin(\beta)} \left[\frac{1 - \exp\left(-\alpha_1 nd - \frac{\alpha_2 nd}{\sqrt{1-t^2}}\right)}{\alpha_1 \sqrt{1-t^2} + \alpha_2} \right. \\
 & \left. + \frac{\exp\left(-\frac{\alpha_2 nd}{\sqrt{1-t^2}}\right) - \exp(-\alpha_1 nd)}{\alpha_1 \sqrt{1-t^2} - \alpha_2} \right] dt
 \end{aligned}$$

where d is the film thickness and β represents the angle of total internal reflection. For SS thin film, $\sin(\beta)$ equals to 1/1.5 (the ratio of the refractive index of air to PVA), while for IPS thin film, it is unity because all the light is believed to be extracted out of the film. By the aid of the above formula, the calculated QY is obtained with $\alpha_1 n = 0.15$ and $\alpha_2 n = 0.06$ with different film thicknesses, in agreement with the experimental results shown in figure 4(b). The formula also yields a well-fitted calculating result of QY (figure 4(c)) under different excitations, by using the experimental thickness of 30 μm and altered α_1 according to the absorption data of the film in figure 3(b). As proved, the QY deviation along with the concentration, thickness and excitation wavelength, to some extent, is affected by the extinction coefficient of the light; and the key to QY enhancement in IPS films lies in the weakening of total internal reflection and the aggregation-induced PL quenching. The above conclusion is also supported by control experiments when using other luminescent materials to prepare the films, such as urea-made C-dots [23] and fluorescent calibration sample, quinine sulfate. As shown in table 1, compared to SS film, IPS film embedded C-dots or quinine sulfate exhibits an apparent QY predominance, with the value almost equivalent to the QY of the counter-original aqueous solution. These experiments confirm our method is a facile and general approach to fabricate large-area freestanding luminescent composite film with liquid-comparably high PL QY.

4. Conclusions

In summary, we realized a freestanding large-area C-dots/PVA composite film with high QY by patterning inverted-pyramid

structure on the surface via a facile template method. Both theoretical calculation and control experiments have demonstrated that the C-dots/PVA composite films with IPS not only suppress the further particle aggregation-induced PL quenching, but weaken the waveguide effect. The strategy finally yields a dramatically enhanced QY of 72.3% by optimizing the geometrical optics, instead of chemical treatment. This method provides a helpful exploration for the application of C-dots in optoelectronic devices, and also a general approach to fabricate large-area freestanding luminescent composite film with liquid-comparably high QY.

Acknowledgments

This work was supported by the National Natural Science Foundation of China (Grant Nos. 11304197 and 61234005).

References

- [1] Baker M 2010 *Nat. Methods* **7** 957
- [2] Shirasaki Y, Supran G J, Bawendi M G and Bulovic V 2013 *Nat. Photon.* **7** 13–23
- [3] Kovalenko M V et al 2015 *ACS Nano* **9** 1012–57
- [4] Yang S T, Cao L, Luo P G, Lu F, Wang X, Wang H, Mezziani M J, Liu Y, Qi G and Sun Y P 2009 *J. Am. Chem. Soc.* **131** 11308–9
- [5] Luo P G, Sahu S, Yang S T, Sonkar S K, Wang J, Wang H, LeCroy G E, Cao L and Sun Y P 2013 *J. Mater. Chem. B* **1** 2116–27
- [6] De B and Karak N 2013 *Rsc Adv.* **3** 8286–90
- [7] Baker S N and Baker G A 2010 *Angew. Chem., Int. Ed.* **49** 6726–44
- [8] Liang Q, Ma W, Shi Y, Li Z and Yang X 2013 *Carbon* **60** 421–8
- [9] Wang X, Qu K, Xu B, Ren J and Qu X 2011 *J. Mater. Chem.* **21** 2445–50
- [10] Sun Y P et al 2006 *J. Am. Chem. Soc.* **128** 7756–7
- [11] Li H, Kang Z, Liu Y and Lee S T 2012 *J. Mater. Chem.* **22** 24230–53
- [12] Zhu S, Meng Q, Wang L, Zhang J, Song Y, Jin H, Zhang K, Sun H, Wang H and Yang B 2013 *Angew. Chem., Int. Ed.* **52** 3953–7
- [13] Lim S Y, Shen W and Gao Z 2015 *Chem. Soc. Rev.* **44** 362–81
- [14] Li X, Zhang S, Kulinich S A, Liu Y and Zeng H 2014 *Sci. Rep.* **4** 4976
- [15] Kwon W, Lee G, Do S, Joo T and Rhee S W 2014 *Small* **10** 506–13
- [16] Kim J Y, Voznyy O, Zhitomirsky D and Sargent E H 2013 *Adv. Mater.* **25** 4986–5010
- [17] Sun M, Qu S, Hao Z, Ji W, Jing P, Zhang H, Zhang L, Zhao J and Shen D 2014 *Nanoscale* **6** 13076–81
- [18] Zhou L, He B and Huang J 2013 *Chem. Commun.* **49** 8078–80
- [19] Kwon W, Do S, Lee J, Hwang S, Kim J K and Rhee S W 2013 *Chem. Mater.* **25** 1893–9
- [20] Jiang Z C, Lin T N, Lin H T, Talite M J, Tzeng T T, Hsu C L, Chiu K P, Lin C A J, Shen J L and Yuan C T 2016 *Sci. Rep.* **6** 19991
- [21] Wang Y, Kalytchuk S, Wang L, Zhovtiuk O, Cepe K, Zboril R and Rogach A L 2015 *Chem. Commun.* **51** 2950–3
- [22] Zhang W, Yu S F, Fei L, Jin L, Pan S and Lin P 2015 *Carbon* **85** 344–50

- [23] Qu D, Zheng M, Zhang L, Zhao H, Xie Z, Jing X, Haddad R E, Fan H and Sun Z 2014 *Sci. Rep.* **4** 5294
- [24] Song Y, Zhu S, Xiang S, Zhao X, Zhang J, Zhang H, Fu Y and Yang B 2014 *Nanoscale* **6** 4676–82
- [25] Han X, Zhong S, Pan W and Shen W 2015 *Nanotechnology* **26** 065402
- [26] Vazsonyi E, De Clercq K, Einhaus R, Van Kerschaver E, Said K, Poortmans J, Szlufcik J and Nijs J 1999 *Sol. Energy Mater. Sol. Cells* **57** 179–88
- [27] Cho H K *et al* 2006 *Opt. Express* **14** 8654–60
- [28] Ishihara K, Fujita M, Matsubara I, Asano T, Noda S, Ohata H, Hirasawa A, Nakada H and Shimoji N 2007 *Appl. Phys. Lett.* **90** 111114
- [29] Jeong S M, Araoka F, Machida Y, Ishikawa K, Takezoe H, Nishimura S and Suzuki G 2008 *Appl. Phys. Lett.* **92** 083307
- [30] Koo W H, Jeong S M, Araoka F, Ishikawa K, Nishimura S, Toyooka T and Takezoe H 2010 *Nat. Photon.* **4** 222–6
- [31] Seo T H, Oh T S, Lee Y S, Jeong H, Kim J D, Kim H, Park A H, Lee K J, Hong C H and Suh E K 2010 *Japan. J. Appl. Phys.* **49** 092101
- [32] Baker-Finch S C and McIntosh K R 2013 *Prog. Photovolt., Res. Appl.* **21** 960–71
- [33] Fashina A A, Adama K K, Oyewole O K, Anye V C, Asare J, Zebaze Kana M G and Soboyejo W O 2015 *J. Renew. Sustain. Energy* **7** 063119